

See discussions, stats, and author profiles for this publication at: <https://www.researchgate.net/publication/276148789>

Atomic Force Microscopy and Voltammetric Investigation of Quadruplex Formation between a Triazole-Acridine Conjugate and Guanine-Containing Repeat DNA Sequences

ARTICLE *in* ANALYTICAL CHEMISTRY · MAY 2015

Impact Factor: 5.64 · DOI: 10.1021/acs.analchem.5b00743 · Source: PubMed

CITATION

1

READS

47

7 AUTHORS, INCLUDING:



AMC Paquim

University of Coimbra

43 PUBLICATIONS 737 CITATIONS

[SEE PROFILE](#)



Ana Dora Pontinha

University of Coimbra

13 PUBLICATIONS 70 CITATIONS

[SEE PROFILE](#)



Ramon Eritja

Spanish National Research Council

376 PUBLICATIONS 7,047 CITATIONS

[SEE PROFILE](#)



Ana Maria Oliveira-Brett

University of Coimbra

233 PUBLICATIONS 5,156 CITATIONS

[SEE PROFILE](#)

¹ Atomic Force Microscopy and Voltammetric Investigation of ² Quadruplex Formation between a Triazole-Acridine Conjugate and ³ Guanine-Containing Repeat DNA Sequences

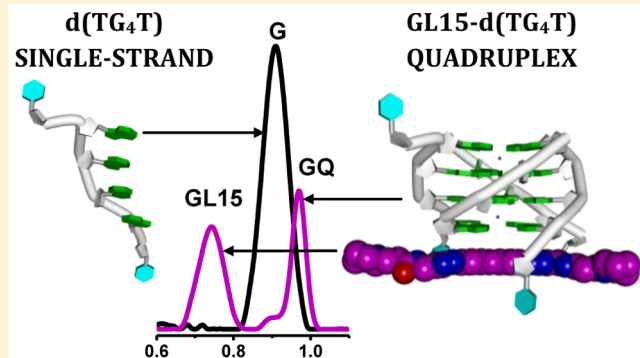
⁴ Ana-Maria Chiorcea-Paquim,[†] Ana Dora Rodrigues Pontinha,[†] Ramon Eritja,[‡] Genny Lucarelli,[§]
⁵ Silvia Sparapani,[§] Stephen Neidle,[§] and Ana Maria Oliveira-Brett^{*,†}

⁶ [†]Department of Chemistry, University of Coimbra, 3004-535 Coimbra, Portugal

⁷ Institute for Research in Biomedicine, IQAC-CSIC, CIBER-BBN Networking Centre on Bioengineering, Biomaterials and
8 Nanomedicine, Barcelona, Spain

⁹ UCL School of Pharmacy, University College London, London WC1N 1AX, U.K.

ABSTRACT: The interactions of the *Tetrahymena* telomeric repeat sequence d(TG₄T) and the polyguanylic acid (poly-(G)) sequence with the quadruplex-targeting triazole-linked acridine ligand GL15 were investigated using atomic force microscopy (AFM) at a highly oriented pyrolytic graphite and voltammetry at a glassy carbon electrode. GL15 interacted with both sequences, in a time dependent manner, and G-quadruplex formation was detected. AFM showed the adsorption of quadruplexes as small d(TG₄T) and poly(G) spherical aggregates and large quadruplex-based poly(G) assemblies, and voltammetry showed the decrease and disappearance of GL15 and guanine oxidation peak currents and appearance of the G-quadruplex oxidation peak. The GL15 molecule strongly stabilized and accelerated G-quadruplex formation in both Na⁺ and K⁺ ion-containing solution, although only K⁺ promoted the formation of perfectly aligned tetra-molecular G-quadruplexes. The small-molecule complex with the d(TG₄T) quadruplex is discrete and approximately globular, whereas the G-quadruplex complex with poly(G) is formed at a number of points along the length of the polynucleotide, analogous to beads on a string.



The telomeres are responsible for the protection of the chromosomes ends, being involved in more than 80% of all cancers. One of the key steps in human carcinogenesis is the activation of the telomeres maintenance system that allows the continued proliferation of cancer cells.

G-quadruplexes (GQs) are four-stranded higher-order structures formed by folding of a single (intramolecular) or by the intermolecular association of two, three, or four separate guanine rich DNA strands.^{1–7} The core motif of the GQ is the G-quartet, a planar grouping of four G bases held together by eight Hoogsteen hydrogen bonds. G-quartets self-associate by $\pi-\pi$ hydrophobic stacking interactions, which are further stabilized by the presence of monovalent cations, notably sodium and potassium, which coordinate the O6 substituent atom of each guanine base and form a cation channel in the interior of a GQ structure. The occurrence of GQ sequences in telomeres, promoter regions, and other genomic locations^{8,9} was determined by the direct visualization of GQ formation in cell nuclei, in the cytoplasm, and at telomeres,^{10,11} which revealed the crucial role of these structures as targets for anticancer drugs.

A large number of potent GQ-binding ligands which stabilize or promote GQ formation have been described in the literature.^{12–15} The GQ ligands in telomeres prevent GQ from unwinding and opening the telomeric ends to telomerase, thus indirectly targeting the telomerase enzyme complex and inhibiting its catalytic activity. Some GQ ligands have shown significant telomerase inhibition or suppression of the transcription activity of oncogenes, thus entering in clinical trials for cancer therapy.

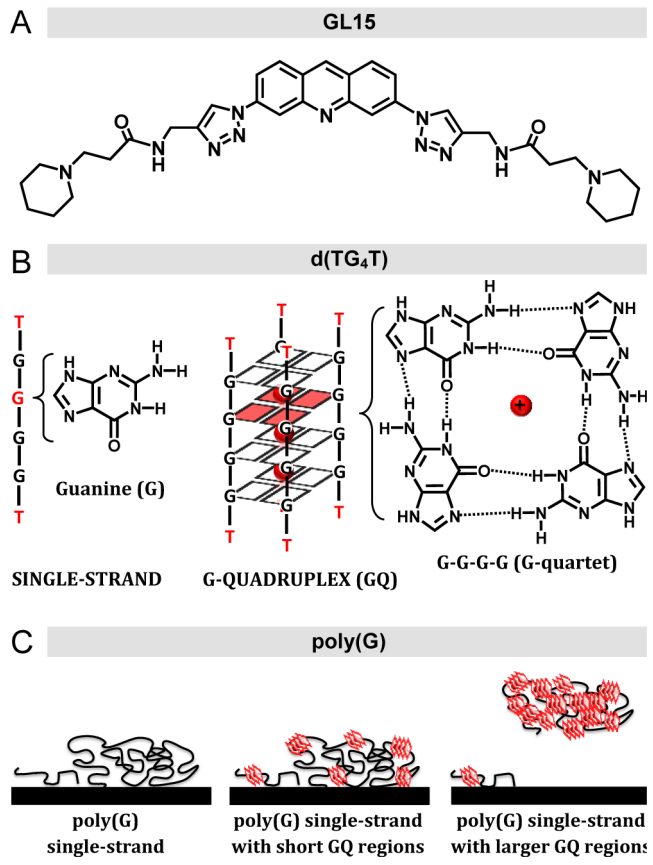
Acridines are heterocyclic compounds some of which have been used as chemotherapeutic agents in human cancer. A number of acridine derivatives have been specifically synthesized with the purpose of increasing binding affinity and selectivity for human telomeric DNA quadruplexes.^{16–20} In particular, the GQ-targeting acridine derivatives BRACO-19 and RHPS4 have been important tools for studying the antitumor activity of this general class of agents. However, they are relatively non GQ-selective, having also significant binding

Received: February 24, 2015

Accepted: May 11, 2015

affinity for duplex DNA.¹⁸ More recently, a series of triazole-linked acridine ligands, e.g., GL15 (Scheme 1A), with enhanced selectivity for human telomeric GQs binding versus duplex DNA binding have been designed, synthesized, and evaluated.¹⁹

Scheme 1. Schematic Representations: (A) the Triazole-Acridine Conjugate GL15, (B) d(TG₄T) in Single-Stranded and in G-Quadruplex Configurations, and (C) the Poly(G) Adsorption Process



DNA-electrochemical biosensors are important tools for the detection and evaluation of small molecule specific binding to nucleic acids,^{21–25} due to their high sensitivity for the detection of small perturbations of DNA morphology. The morphological characteristics of DNA molecules in GQ configurations have been recently investigated at carbon electrodes,^{26–33} from the viewpoint of nanotechnology and biosensor technology applications.

The triazole-acridine conjugate compound GL15 has been investigated by voltammetric techniques, providing new data concerning its interaction with duplex DNA.³⁴

The *Tetrahymena* telomeric repeat sequence d(TG₄T) (Scheme 1B) forms parallel-stranded tetra-molecular GQs in the presence of Na⁺ and K⁺ ions³⁵ and is considered to be a simple model for biologically relevant GQs. It has also provided high-resolution structural data on drug–DNA interactions.^{36,37} Synthetic polynucleotides poly(dG) and poly(G) are also widely used as models to determine the interaction of drugs with G-rich segments of DNA.

The analytical characterization of the binding process between GQ ligands and GQ regions of DNA, without any labeling is crucial and emerges as a necessary step for the

development of new sensitive GQ-based biosensor devices for cancer diagnosis and treatment.

This paper reports an exhaustive qualitative analytical study on the interactions of the short-length sequence d(TG₄T) and long polyguanylic acid (poly(G)) sequence with the triazole-acridine conjugate GL15, using a novel approach, based on the combination of two powerful analytical techniques, atomic force microscopy (AFM) onto a highly oriented pyrolytic graphite (HOPG) surface and differential pulse (DP) voltammetry at a glassy carbon electrode (GCE). The interaction of GL15 with d(TG₄T) and poly(G) was evaluated based on changes in structure and redox behavior, enhanced by the presence of Na⁺ or K⁺ ions. The insights into the molecular basis of the GQ formation by GL15 will provide new opportunities for therapeutic intervention in a wide variety of human cancers, including leukemia, lymphomas, and most carcinomas, and it will trigger the future use of these combined analytical techniques.

MATERIALS AND METHODS

Materials and Reagents. The 6-mer single-stranded hexadeoxyribonucleotide sequence 5'-TGGGGT-3' (d(TG₄T)) was synthesized on an Applied Biosystems 380B automated DNA synthesizer using reagents for oligodeoxyribonucleotides chemistry (Fluka, Germany). The d(TG₄T) purity was verified by NMR and high-pressure liquid chromatography (HPLC) analysis. Polyguanylic acid (poly(G)) purchased from Sigma-Aldrich was used without further purification.

The triazole-acridine conjugate GL15 *N,N'*-((1,1'-(acridine-3,6-diyl)bis(1H,1,2,3-triazole-4,1-diyl))bis(methylene))bis(2-piperidin-1-yl)propanamide was synthesized and purified by the previously described methods.¹⁹

The supporting electrolyte solution was 0.1 M phosphate buffer pH = 7.0, containing Na⁺ ions (0.2 M NaH₂PO₄ + 0.2 M Na₂HPO₄) or K⁺ ions (0.2 M KH₂PO₄ + 0.2 M K₂HPO₄), prepared using analytical grade reagents and purified water from a Millipore Milli-Q system, with conductivity <0.1 μS cm⁻¹.

The d(TG₄T) control and GL15-d(TG₄T) stock solutions were prepared using 3.0 μM d(TG₄T) incubated in the absence/presence of 4.0 μM GL15, in supporting electrolyte. The poly(G) control and GL15-poly(G) stock solutions were prepared using 100 μg mL⁻¹ poly(G) incubated in the absence/presence of 4.0 μM GL15 in supporting electrolyte. All experiments were done at room temperature (25 ± 1 °C).

Synthetic Chemistry. To a suspension of *N*-(prop-2-yn-1-yl)-3-(piperidin-1-yl)propanamide (0.31 g, 1.60 mmol) and 3,6-diazoacridine (0.20 g, 0.77 mmol) in tBuOH (2 mL), a solution of (+)-sodium L-ascorbate (0.076 g, 0.38 mmol) and copper(II) sulfate pentahydrate (0.019 g, 0.077 mmol) in H₂O (2 mL) was added in one portion. The heterogeneous mixture was treated according to the general procedure to afford a brown solid (0.047 g, 28%).¹⁹

Atomic Force Microscopy (AFM). AFM was performed in the acoustic ac mode, with a PicoScan controller and a CS AFM S scanner with a scan range of 6 μm in *x*–*y* and 2 μm in *z* (Agilent Technologies). AppNano type FORT of 225 μm length, 3.0 N m⁻¹ spring constants and 47–76 kHz resonant frequencies in air (Applied NanoStructures, Inc.) were used. All AFM images were topographical and were taken with 512 samples/line × 512 lines and scan rates of 0.8–2.5 lines s⁻¹.

HOPG, grade ZYB of $15 \times 15 \times 2$ mm³ dimensions (Advanced Ceramics Co.) was used as a substrate in the AFM study, because is atomically flat with less than 0.06 nm of root-mean-square (r.m.s.) roughness for a 1000×1000 nm² surface area. The GCE used for the voltammetric characterization is much rougher, with 2.10 nm r.m.s. roughness for the same surface area, therefore unsuitable for AFM surface characterization. The electrochemical experiments showed similar redox behavior using GCE and HOPG.

For each incubation time investigated by AFM, the d(TG₄T) control and GL15-d(TG₄T) stock solutions were diluted in buffer to 0.3 μ M d(TG₄T) without/with 0.4 μ M GL15, and the poly(G) control and GL15-poly(G) stock solutions were diluted in buffer to 5.0 μ g mL⁻¹ poly(G) without/with 0.2 μ M GL15, in order to maintain the same d(TG₄T):GL15 and poly(G):GL15 ratios in the AFM and voltammetric experiments.

The HOPG surfaces were modified by spontaneous adsorption of d(TG₄T) control, GL15-d(TG₄T), poly(G) control, and GL15-poly(G), after depositing 100 μ L of each solution onto the freshly cleaved HOPG, over a period of 3 min. The solution excess was gently cleaned with Milli-Q water, and the HOPG with the adsorbed molecules was then dried in a sterile atmosphere and imaged by AFM in air. This procedure provided reproducible qualitative analytical results when compared with AFM in solution, when the adsorption of molecules continued to occur during the AFM experiments and made it difficult for the surface coverage comparison.

AFM images of DNA investigated in air and under water showed similar patterns of adsorption.³⁸ Furthermore, the GQs pattern of adsorption is expected to be maintained at even a higher degree after drying, since GQs are much stiffer, compact, and robust when compared with single-and double-stranded DNA. In addition, the d(TG₄T) and poly(G) stability on the hydrophobic HOPG surface and their mechanical properties, such as stiffness and hardness, under dry conditions are higher when compared to wet conditions,³⁹ which ensure the reproducibility of the results.

Voltammetric Experiments. Voltammetry was carried out using a μ Autolab Type II potentiostat running with GPES 4.9 software (Metrohm-Autolab, The Netherlands). DP voltammetry conditions were pulse amplitude 50 mV, pulse width 70 ms, and scan rate 5 mV s⁻¹. Measurements were carried out using a GCE working ($d = 1$ mm), a Pt wire counter, and an Ag/AgCl (3 M KCl) reference electrodes, in a one-compartment 2 mL electrochemical cell.

Before every electrochemical assay, the GCE was polished using diamond spray (particle size 1 μ m), rinsed with Milli-Q water, placed in buffer supporting electrolyte, and various DP voltammograms were recorded until a steady state baseline voltammogram was obtained.

For each incubation time investigated, DP voltammograms of d(TG₄T) control, GL15-d(TG₄T), poly(G) control, and GL15-poly(G) stock solutions were obtained. The GCE was always cleaned by polishing between measurements, to avoid misleading results from the d(TG₄T), poly(G), or GL15 adsorption. The DP voltammograms were baseline corrected using the moving average with a step window of 2 mV included in the GPES (version 4.9) software.

RESULTS

Interaction of d(TG₄T) with GL15. The d(TG₄T) contains one block of four contiguous guanine residues which

can form a parallel-stranded tetra-molecular GQ, stabilized by $\pi-\pi$ interactions between the G-quartets and to some extent by the thymine residues present at the 5' and 3' ends (Scheme 1B). The mechanism of interaction between GL15 and d(TG₄T) to form a GL15-d(TG₄T) complex and the influence of GL15 on GQ formation and stabilization have been investigated. For control and a correct evaluation of structural changes in d(TG₄T) after interaction with GL15, the GL15 and d(TG₄T) control adsorption patterns and redox behavior were also studied.

AFM Characterization. The GL15 and d(TG₄T) controls and GL15-d(TG₄T) films were obtained by spontaneous adsorption onto HOPG, as described in the Atomic Force Microscopy (AFM) section.

GL15 and d(TG₄T) Control. AFM images of the GL15 control, for 0.2 μ M and 0.4 μ M (Figure 1A), the concentrations

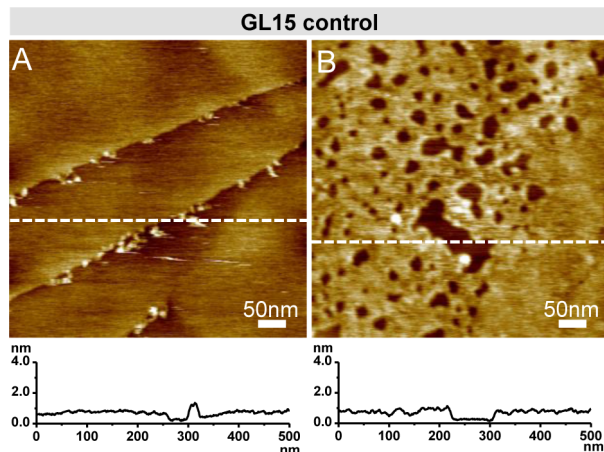


Figure 1. AFM images and cross-section profiles through the white dotted lines: GL15 control at (A) 0.4 μ M and (B) 4.0 μ M.

used in the AFM study, and for 4.0 μ M (Figure 1B), the concentration used in the voltammetric study, showed different adsorption coverages. AFM images of 0.2 μ M and 0.4 μ M GL15 control showed very weak adsorption onto HOPG, suggesting negligible nonspecific adsorption of GL15, whereas AFM images of 4.0 μ M GL15 control showed almost complete HOPG coverage by a smooth film, 0.70 \pm 0.05 nm height, corresponding to the adsorption of a self-assembled GL15 monolayer, with the acridine moieties lying flat on the surface.

The d(TG₄T) control adsorption pattern was obtained in 0.3 μ M d(TG₄T) in the presence of Na⁺ or K⁺ ions, at different times. AFM images of the d(TG₄T) control in freshly prepared solutions (Figure 2A in Na⁺ and Figure 2B in K⁺ ions) showed only the d(TG₄T) single-strand adsorption, detected as 0.87 \pm 0.1 nm height randomly oriented polymeric structures (rP, random polymer).

On increasing the d(TG₄T) control time from 0 to 42 days (Figure 3A,B in Na⁺ and Figure 3C in K⁺ ions), the d(TG₄T) single-strands started to self-assemble into short tetra-molecular d(TG₄T)-GQ complexes (Scheme 1B). The AFM images showed (i) the decrease and disappearance of the rP structures, due to a decrease in the number of d(TG₄T) single strands, (ii) the occurrence and the increase of a number of small 2.05 \pm 0.5 nm height spherical aggregates (A, aggregates), due to the adsorption of d(TG₄T)-GQs, and (iii) in Na⁺ containing solutions, the occurrence of a few 1.52 \pm 0.4 nm height polymeric nanostructures (N, nanostructures).

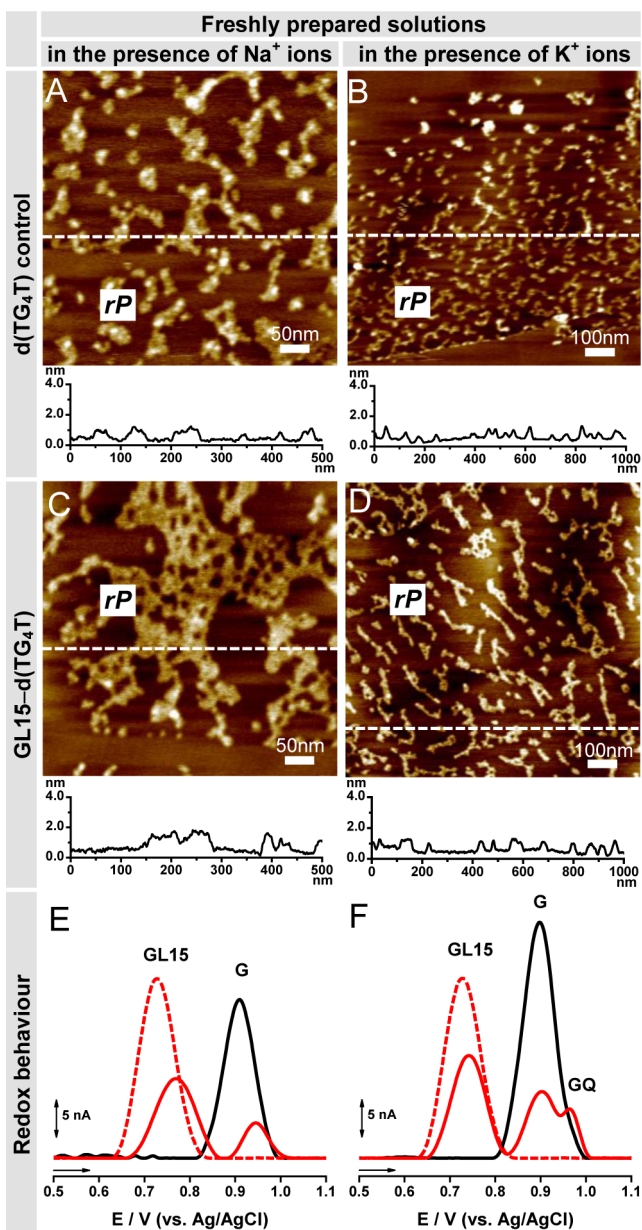


Figure 2. Freshly prepared solutions. AFM images and cross-section profiles through the white dotted lines: (A, B) d(TG₄T) control and (C, D) GL15-d(TG₄T), in the presence of (A, C) Na⁺ and (B, D) K⁺ ions. DP voltammograms baseline corrected: (black —) d(TG₄T) control, (red ...) GL15 control, and (red —) GL15-d(TG₄T), in the presence of (E) Na⁺ and (F) K⁺ ions.

The presence of K⁺ ions has stabilized and accelerated GQ formation, and after 42 days incubation in K⁺ ions only, d(TG₄T)-GQ complexes are observed (Figure 3C), when compared with Na⁺ ions, where d(TG₄T) single-stranded species are still present (Figure 3A).

GL15-d(TG₄T) Interaction. The GL15-d(TG₄T) interaction was investigated using a solution of 3.0 μ M d(TG₄T) incubated with 0.4 μ M GL15 for a range of incubation times, in the presence of Na⁺ or K⁺ ions. This procedure led to the coadsorption of GL15-d(TG₄T) complexes together with free d(TG₄T) and GL15 molecules.

AFM images of GL15-d(TG₄T) freshly prepared solutions showed only rP structures, 0.92 \pm 0.10 nm height in the presence of Na⁺ ions (Figure 2C) and 0.89 \pm 0.1 nm height in

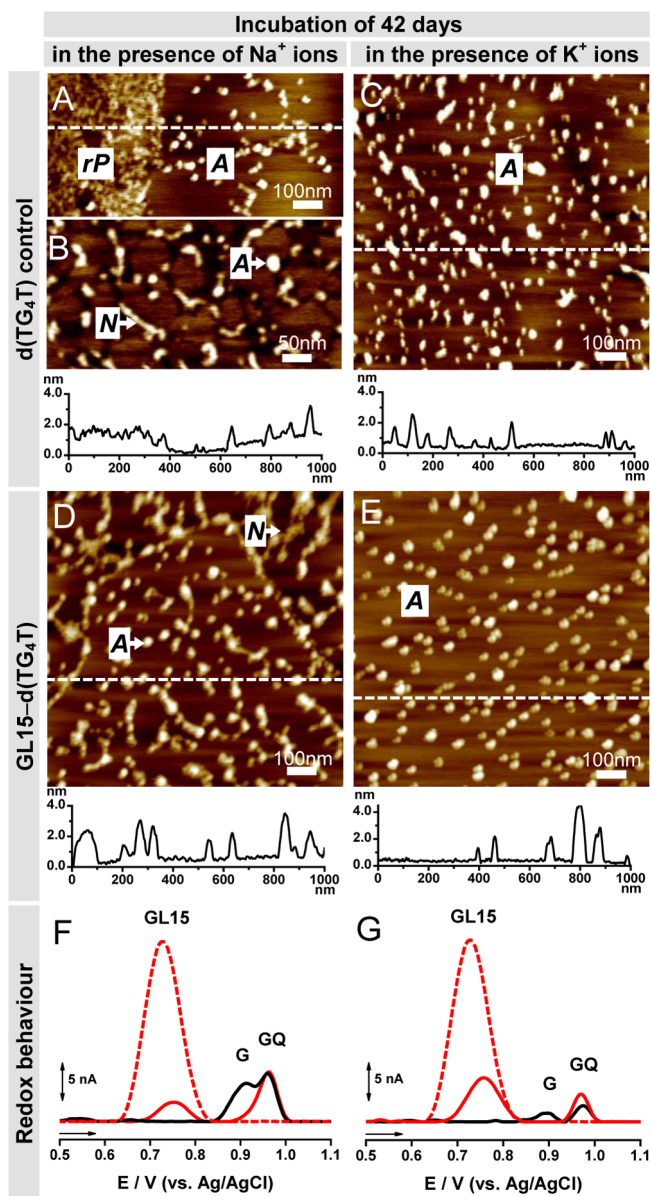


Figure 3. Incubation for 42 days. AFM images and cross-section profiles through the white dotted lines: (A, B, C) d(TG₄T) control and (D, E) GL15-d(TG₄T), in the presence of (A, B, D) Na⁺ and (C, E) K⁺ ions. DP voltammograms baseline corrected: (black —) d(TG₄T) control, (red ...) GL15 control, and (red —) GL15-d(TG₄T), in the presence of (G) Na⁺ and (F) K⁺ ions.

the presence of K⁺ ions (Figure 2D), due to the adsorption of GL15-d(TG₄T) and d(TG₄T) single-stranded species, similar to what was previously observed for d(TG₄T) in freshly prepared solutions (Figure 2A with Na⁺ and Figure 2B with K⁺ ions).

Increasing the GL15-d(TG₄T) incubation time from 0 to 42 days (Figure 3D in Na⁺ and Figure 3E in K⁺ ions) results in the d(TG₄T) single strands self-assembling into d(TG₄T)-GQs both with and without bound GL15. The AFM images showed (i) the decrease and the disappearance of the rP structures, due to a decrease in the number of available d(TG₄T) single strands, (ii) the occurrence and increase of the 2.32 \pm 0.6 nm height A aggregates corresponding to GQ adsorption, and (iii) the occurrence of 1.52 \pm 0.4 nm height N nanostructures in the presence of Na⁺ ions.

288 The GQ height measured in AFM images is similar to the
 289 ~2.6 nm diameter measured by X-ray crystallography.³⁵ The
 290 GQ structures formed by GL15-d(TG₄T) and d(TG₄T)
 291 interacted and adsorbed less on the hydrophobic HOPG,
 292 because they have the guanine bases buried in the interior of
 293 the structures, protected by the sugar-phosphate backbones,
 294 when compared with the single-stranded unfolded structures
 295 with bases more exposed and freer to undergo hydrophobic
 296 interactions with the carbon surface.⁴⁰

297 After 42 days incubation of GL15-d(TG₄T) in the presence
 298 of Na⁺ ions, no single strands were observed (Figure 3D), when
 299 compared with d(TG₄T) control (Figure 3A), demonstrating
 300 that GL15 binding to d(TG₄T) accelerated the formation of
 301 GQ-ligand complexes.

302 The formation of d(TG₄T) higher-order N nanostructures
 303 was observed only in solutions containing Na⁺ ions for long
 304 incubation times, independent of the presence of GL15 in
 305 solution. The presence of K⁺ ions promoted the rapid
 306 formation of stable and perfectly aligned tetra-molecular GQs,
 307 and consequently higher-order nanostructures did not form.

308 *Voltammetric Characterization. GL15 and d(TG₄T) Control.* DP voltammograms in 4.0 μM GL15 control showed the
 309 occurrence of one GL15 oxidation peak, at $E_{pa} = +0.77$ V
 310 (Figures 2E,F (red ...) and 3F,G (red ...)).

311 The d(TG₄T) control redox behavior was investigated in
 312 solutions of 3.0 μM d(TG₄T) in the presence of Na⁺ or K⁺
 313 ions, at different times. DP voltammograms of d(TG₄T)
 314 control in freshly prepared solutions (Figure 2E (black —)) in
 315 Na⁺ and Figure 2F (black —) in K⁺ ions) showed the
 316 occurrence of only one G oxidation peak, due to the oxidation
 317 of the guanine residues in the d(TG₄T) single strands (Scheme
 318 1B, left), at the C₈-H position, in a two-step mechanism each
 319 involving two electrons and two proton transfers.⁴¹

320 On increasing the d(TG₄T) control time from 0 to 42 days
 321 (Figure 3F (black —) in Na⁺ and Figure 3G (black —) in K⁺
 322 ions), the d(TG₄T) single strands started to self-assemble into
 323 d(TG₄T)-GQs (Scheme 1B, right).⁴¹ The DP voltammograms
 324 showed (i) a decrease in the guanine (G) oxidation peak
 325 current and (ii) occurrence and increase of the GQ oxidation
 326 peak current, due to the oxidation of the guanine residues in the
 327 d(TG₄T)-GQs that were formed.

328 The G oxidation peak current decrease is due to a decrease in
 329 the number of guanine residues in the d(TG₄T) single strands,
 330 and the GQ oxidation peak current increase is due to an
 331 increase in the overall number of GQs. The GQ oxidation peak
 332 potential is higher relative to the G oxidation peak potential,
 333 due to the greater distance for the electron transfer from the
 334 interior of the rigid GQs to the GCE surface, than from the
 335 more flexible d(TG₄T) single strands. The oxidation of
 336 thymine residues in d(TG₄T) is not detected by DP
 337 voltammetry, because it occurs at a much greater positive
 338 potential, near the potential of oxygen evolution.²⁰

339 *GL15-d(TG₄T) Interaction.* The GL15-d(TG₄T) interaction
 340 was investigated in solutions of 3.0 μM d(TG₄T) incubated
 341 with 4.0 μM GL15, in the presence of Na⁺ or K⁺ ions, for a
 342 range of incubation times. The GL15, G, and GQ oxidation
 343 peaks of the GL15-d(TG₄T) complex were compared with the
 344 oxidation peaks of d(TG₄T) and GL15 controls.

345 *Freshly Prepared Solutions.* GL15-d(TG₄T)-GQs formation
 346 in the presence of Na⁺ ions was a slow process. DP
 347 voltammograms of GL15-d(TG₄T) showed the occurrence of
 348 two oxidation peaks (Figure 2E (red —)): (i) the GL15
 349 oxidation peak, at $E_{pa} = +0.77$ V, and (ii) the G oxidation peak,
 350

351 at $E_{pa} = +0.95$ V, corresponding to the d(TG₄T) single strands,
 352 in agreement with the adsorption of solely single-stranded
 353 GL15-d(TG₄T) and d(TG₄T) molecules observed in the AFM
 354 (Figure 2C).

355 GL15-d(TG₄T)-GQs formation in the presence of K⁺ ions
 356 was very rapid. DP voltammograms of GL15-d(TG₄T)
 357 immediately showed the occurrence of three oxidation peaks
 358 (Figure 2F (red —)): (i) the GL15 oxidation peak, at $E_{pa} =$
 359 +0.74 V, (ii) the G oxidation peak of the d(TG₄T) single
 360 strands, at $E_{pa} = +0.90$ V, and (iii) the GQ oxidation peak of the
 361 d(TG₄T)-GQs, at $E_{pa} = +0.97$ V. DP voltammetry of
 362 d(TG₄T)⁴¹ and kinetic studies by absorbance spectroscopy
 363 which monitored association and dissociation of tetra-molecular
 364 GQs formed by oligonucleotides containing more than four
 365 contiguous guanine residues⁴² and also showed more rapid
 366 association in the presence of K⁺ ions.

367 The decrease of the GL15 oxidation peak current of GL15-
 368 d(TG₄T) (Figure 2E,F (red —)), when compared with GL15
 369 control (Figure 2E,F (red ...)), is due to GL15 binding to
 370 d(TG₄T). The decrease of the G oxidation peak current of
 371 GL15-d(TG₄T) (Figure 2E,F (red —)) and the occurrence of
 372 the GQ oxidation peak in K⁺ ions (Figure 2F (red —)), when
 373 compared with d(TG₄T) control, which showed only one large
 374 G oxidation peak (Figure 2E,F (black —)), further
 375 demonstrated that GL15 binding to d(TG₄T) promotes GQ
 376 formation.

377 *Increasing Incubation Times.* The GL15-d(TG₄T) incubation
 378 time dependence is shown in Figure 4. On increasing
 379 GL15-d(TG₄T) incubation time in the presence of Na⁺ ions
 380 from 0 to 42 days (Figure 4A), the DP voltammograms showed

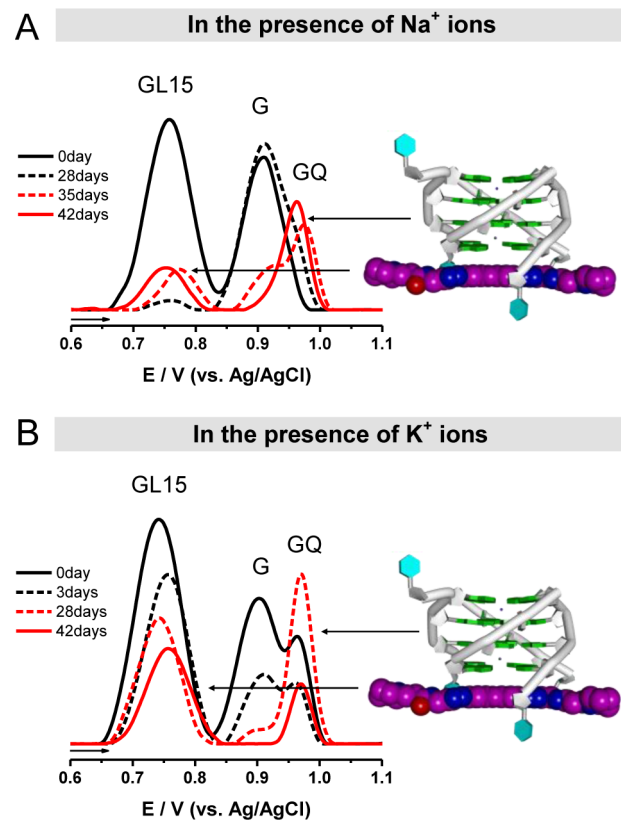


Figure 4. DP voltammograms baseline corrected for GL15-d(TG₄T), with different incubation times in the presence of (A) Na⁺ and (B) K⁺ ions.

(i) a significant decrease in the GL15 oxidation peak current, due to GL15 binding to d(TG₄T) and consequent decrease in the number of free GL15 molecules, (ii) a decrease in the G oxidation peak current due to a decrease in the number of d(TG₄T) single strands, and (iii) the GQ oxidation peak occurrence (Figure 4A (black ...) 28 days incubation) and increase (Figure 4A (red ...) 35 days and (red —) 42 days incubation), due to the formation and stabilization of d(TG₄T)-GQ complexes (Figure 4A, left).

On increasing the GL15-d(TG₄T) incubation time in the presence of K⁺ ions, from 0 to 42 days (Figure 4B), the DP voltammograms showed (i) a decrease in the GL15 oxidation peak current, (ii) a decrease in the G oxidation peak current, and (iii) a progressive increase of the GQ oxidation peak current up to 28 days incubation (Figure 4B (red ...) 28 days incubation), due to the formation and stabilization of d(TG₄T)-GQs (Figure 4B, left), followed by a decrease in the GQ oxidation peak current for 35 and 42 days incubation (Figure 4B (red —)).

The decrease in the GQ oxidation peak current for long incubation times occurred only with GL15-d(TG₄T) in the presence of K⁺ ions (Figure 4B (red —) 42 days incubation) and was not observed in the presence of Na⁺ ions (Figure 4A (red —) 42 days incubation) nor in the d(TG₄T) control with Na⁺ or K⁺ ions. This demonstrated that GL15 binding to d(TG₄T)-GQs in K⁺ ions confers greater structural stability to the very rigid and stable d(TG₄T)-GQs, the transition of electrons from the interior guanines being more difficult. This is in agreement with the AFM results which showed rapid formation of solely GQ structures in solutions containing K⁺ ions (Figure 3E).

The presence of GL15 strongly stabilized and accelerated d(TG₄T)-GQ formation, and after 42 days incubation almost all GL15 was bound only to d(TG₄T)-GQs. Indeed, after 42 days incubation, DP voltammograms of GL15-d(TG₄T) showed small GL15 oxidation peak shoulders and only the GQ oxidation peak was present (Figure 3F (red —) in Na⁺ and Figure 3G (red —) in K⁺ ions), when compared with the d(TG₄T) control which still showed the G oxidation peak of d(TG₄T) single strands (Figure 3F,G (black —)).

In addition, the G oxidation peak of GL15-d(TG₄T) was always smaller compared to the G oxidation peak of the d(TG₄T) control, due to the reduced number of d(TG₄T) single strands in the presence of GL15. The AFM results confirmed that upon increasing the incubation time, GL15-d(TG₄T) complex self-assembled into short GQs (Figure 3D,E). The GL15 acridine chromophore prefers to bind on the terminal G-quartet stacks of the d(TG₄T)-GQs. This is quite distinct from intercalation into the DNA duplex, even though the GL15 extended electron aromatic ring system enables it to form strong π-π stacking interactions with the guanine bases, as observed with a number of small molecule-GQ complexes (see, for example, refs 43–45) the triazole-acridine compounds as a class do not show significant duplex DNA affinity,¹⁹ in contrast to many other substituted acridines.

Interaction of Poly(G) with GL15. AFM Characterization. The deposited films of poly(G) control and GL15-poly(G) were obtained by spontaneous adsorption onto HOPG, using solutions of 5.0 μg mL⁻¹ poly(G) incubated in the presence and absence of 0.2 μM GL15, with Na⁺ or K⁺ ions, for different time periods.

Poly(G) Control. AFM images of the poly(G) control in freshly prepared solutions (Figure 5A in Na⁺ and Figure 5B in

K⁺ ions) showed the adsorption of solely poly(G) single-strands (Scheme 1C, left), detected in the AFM images as 0.7 ± 0.1 nm height rP structures. 444 445 446

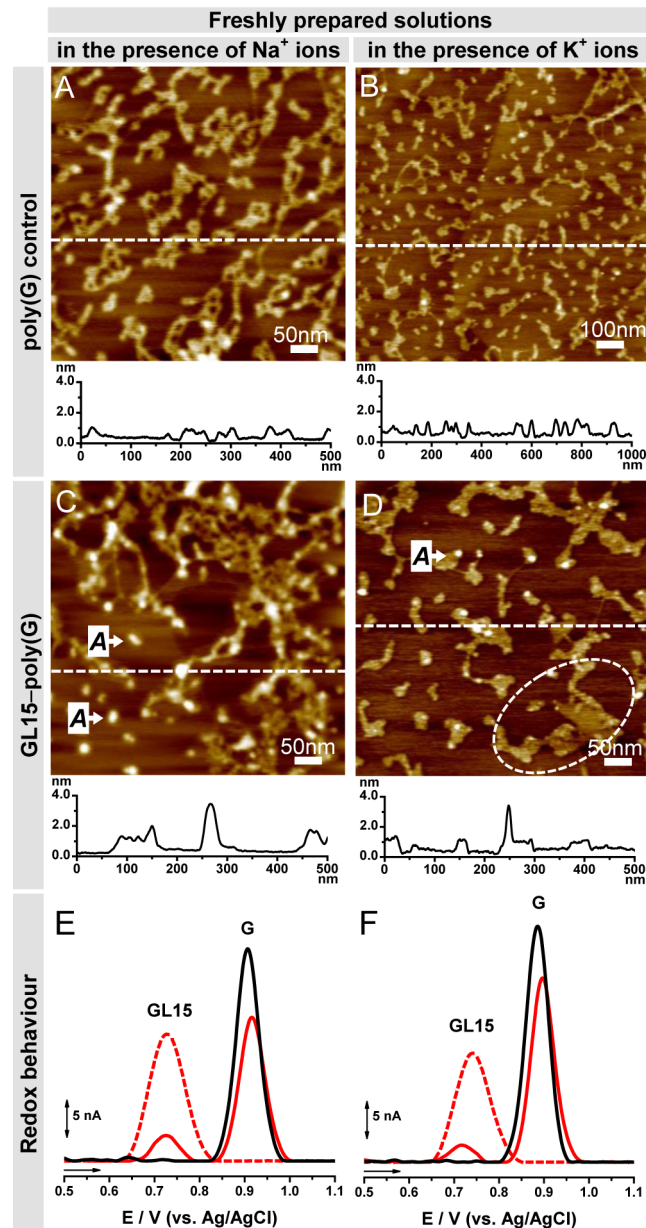


Figure 5. Freshly prepared solutions. AFM images and cross-section profiles through the white dotted lines: (A, B) poly(G) control and (C, D) GL15-poly(G), in the presence of (A, C) Na⁺ and (B, D) K⁺ ions. DP voltammograms baseline corrected: (black —) poly(G) control, (red ...) GL15 control, and (red —) GL15-poly(G), in the presence of (E) Na⁺ and (F) K⁺ ions.

AFM images of poly(G) control with increasing times, from 0 to 28 days, showed (i) a decrease in rP structures due to a decrease in the number of poly(G) single strands, (ii) the occurrence and increase in the number of 2.2 ± 0.3 nm height A spherical aggregates, due to the formation of short GQ regions along the poly(G) single strands, and (iii) for large incubation times (28 days incubation), the formation of compact poly(G) aggregated morphologies in Na⁺ ions (Figure 6A) and a very low pattern of adsorption in K⁺ ions solutions

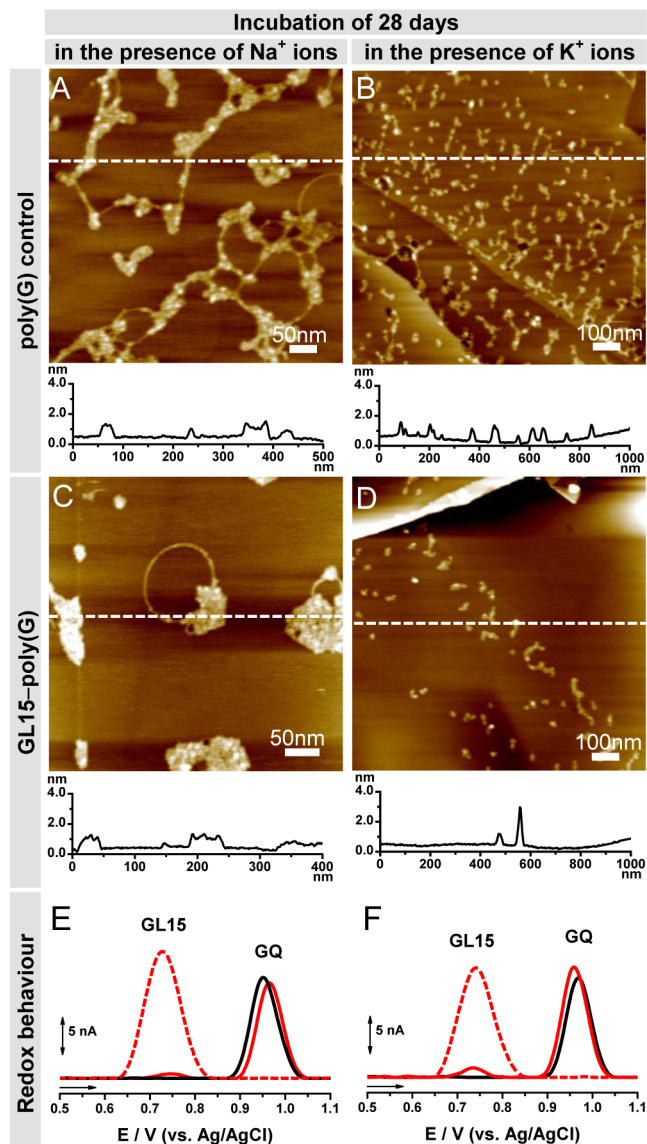


Figure 6. Incubation for 28 days. AFM images and cross-section profiles through the white dotted lines: (A, B) poly(G) control and (C, D) GL15-poly(G), in the presence of (A, C) Na⁺ and (B, D) K⁺ ions. DP voltammograms baseline corrected: (black —) poly(G) control, (red ...) GL15 control, and (red —) GL15-poly(G), in the presence of (E) Na⁺ and (F) K⁺ ions.

(Figure 6B), due to the formation of large poly(G)-GQ assemblies.³² The short poly(G)-GQ regions formed after short incubation times were dragged down to the surface by the larger poly(G) single-strand adsorption onto HOPG (Scheme 1C, middle), while larger poly(G)-GQ assemblies, formed after long incubation times, stayed in solution and had very low adsorption (Scheme 1C, right).

GL15-poly(G) Interaction. AFM images of GL15-poly(G) in freshly prepared solution (Figure 5C in Na⁺ and Figure 5D in K⁺) showed two adsorption morphologies: (i) 0.7 ± 0.1 nm height rP structures due to the adsorption of poly(G) single-strands (Scheme 1C, left) and (ii) a large number of 2.7 ± 0.5 nm height A aggregates, due to the formation of short GQ regions along the poly(G) single-strands (Scheme 1C, middle). Additionally, in K⁺ solution, several GL15-poly(G) molecules started to form compact aggregated morphologies (Figure 5D,

dashed circle). This adsorption pattern was only observed for the poly(G) control with large incubation times, demonstrating that the presence of GL15 accelerates GQ formation and stabilization, as previously observed for d(TG₄T).

On increasing GL15-poly(G) incubation time from 0 to 28 days, the AFM images showed (i) progressive decrease and disappearance of rP structures due to the decrease in the number of GL15-poly(G) single strands, (ii) the occurrence and increase of a number of A spherical aggregates, due to the formation of short discrete GQ regions along the poly(G) single strands, and (iii) some GL15-poly(G) molecules started to form aggregated morphologies.

With long incubation times (28 days incubation), in the presence of Na⁺ ions, the densely condensed GL15-poly(G) molecules formed arrangements resembling diamond rings (Figure 6C), while in the presence of K⁺ ions almost no adsorption occurred (Figure 6D), consistent with the formation of large GL15-poly(G)-GQ aggregates.

GL15-poly(G) had much reduced surface coverage, when compared with the poly(G) control (Figure 6A,B), demonstrating that GL15 binding to poly(G) accelerated GQ formation and stabilization in the presence of both Na⁺ and K⁺ ions.

Voltammetric Characterization. Poly(G) Control. The poly(G) control redox behavior was investigated in solutions of 100 $\mu\text{g mL}^{-1}$ poly(G) in the presence of Na⁺ or K⁺ ions, for different time periods.

DP voltammograms of poly(G) control in freshly prepared solutions (Figure 5E (black —) in Na⁺ and Figure 5F (black —) in K⁺ ions), showed the occurrence of only one G oxidation peak, at $E_{\text{pa}} = +0.90$ V, due to the oxidation of the guanine residues in the poly(G) single strands.³²

On increasing the poly(G) control time from 0 to 28 days (Figure 6E (black —) in Na⁺ and Figure 6E (black —) in K⁺ ions), DP voltammograms showed (i) the decrease and disappearance of the G oxidation peak of the poly(G) single strands and (ii) the occurrence of a GQ oxidation peak, at $E_{\text{pa}} = +0.98$ V, due to the formation and stabilization of poly(G)-GQs.³¹

GL15-poly(G) Interaction. GL15-poly(G) interaction was examined in solutions of 100 $\mu\text{g mL}^{-1}$ poly(G) incubated with 4.0 μM GL15 in the presence of Na⁺ and K⁺ ions, during a range of incubation times, and showed redox behavior similar to that of the GL15-d(TG₄T) interaction. The GL15, G, and GQ oxidation peaks of the GL15-poly(G) complex were compared with the oxidation peaks of poly(G) and GL15 controls.

Freshly Prepared Solutions. DP voltammograms of GL15-poly(G) in freshly prepared solution (Figure 5E (red —) in Na⁺ and Figure 5F (red —) in K⁺ ions) showed two oxidation peaks: (i) the GL15 oxidation peak, at $E_{\text{pa}} = +0.73$ V and (ii) the G oxidation peak, at $E_{\text{pa}} = +0.90$ V, due to oxidation of the guanine residues in the poly(G) single-strands.

A large decrease in the GL15 oxidation peak current compared to the GL15 control took place (Figure 5E,F (red ...)), suggesting that GL15 interacted very rapidly with poly(G), resulting in a decreased number of free GL15 molecules. Reduced G oxidation peak currents were observed for GL15-poly(G) compared with the poly(G) control (Figure 5E (black —) in Na⁺ and Figure 5F (black —) in K⁺ ions). This is due to fewer poly(G) single strands available in the presence of GL15 and is caused by the formation of several short GL15-poly(G)-GQ regions, as observed in the AFM

535 images (Figure 5C,D). The GQ oxidation peak of the GL15-
536 poly(G)-GQ regions was below the DP voltammetry detection
537 limit.

538 *Increasing Incubation Time.* On increasing the GL15-
539 poly(G) incubation time from 0 to 28 days (Figure 6E (red —)
540 in Na⁺ and Figure 6F (red —) in K⁺ ions), the DP
541 voltammograms showed (i) the disappearance of the GL15
542 oxidation peak close to the signal/noise ratio, due to all free
543 GL15 molecules binding to poly(G), (ii) the decrease and
544 disappearance of the G oxidation peak of the GL15-poly(G)
545 single strands, and (iii) the occurrence of the GQ oxidation
546 peak, at $E_{pa} = +0.97$ V, due to the formation and stabilization of
547 GL15-poly(G)-GQ complexes.

548 The phase of poly(G) single strand self-assembly started with
549 the generation of short GQ regions. These increased with
550 incubation time, after which they started to fold into larger
551 aggregates containing GQs, with the guanine residues more
552 difficult to oxidize, shown by the smaller GQ oxidation peaks.

553 The GQ oxidation peak of the GL15-poly(G)-GQ after 28
554 days incubation (Figure 6E (red —) Na⁺ and Figure 6F (red
555 —) K⁺ ions) occurred at the same potential of the GQ
556 oxidation peak of GL15-d(TG₄T)-GQ_t at $E_{pa} = +0.97$ V,
557 (Figure 4A (black ...) in Na⁺ and Figure 4B (red ...) in K⁺
558 ions).

559 ■ DISCUSSION

560 GQ formation has been extensively studied in a variety of
561 telomeric and other guanine-rich sequences. The d(TG₄T)
562 sequence has been used as a model system for telomeric DNA
563 in higher organisms, and both crystallographic and NMR
564 structural data have shown that small molecules, such as the
565 anticancer drug daunomycin, bind to one face of the
566 tetramolecular d(TG₄T) parallel quadruplex.³⁶ The present
567 AFM data is entirely consistent with these findings with the
568 phosphate-phosphate interstrand distances found by X-ray
569 crystallography of ~2.6 nm remarkably close to those found by
570 AFM. A molecular model for the GL15-d(TG₄T) parallel
571 quadruplex (Figure 4) shows that the nonintercalative end-
572 stacking binding of GL15 has not altered the cross-diameter
573 dimension of the GQ.

574 There is little data available on small-molecule binding to
575 poly(G) sequences, although such sequences are widely
576 prevalent in the human and other genomes at both DNA and
577 RNA levels. Fiber diffraction data on poly(G) has shown that in
578 K⁺ solution it consists of a continuous 4-fold helix,⁴⁶ whose
579 regularity may well be a consequence of the process of forming
580 a polynucleotide fiber. Recent NMR studies⁴⁷ have shown that
581 short lengths of poly(G) can form discrete GQ structures, with
582 parallel topology and propeller loops, strikingly similar in form
583 to the GQs formed by human telomeric DNA and RNA
584 sequences in conditions of high concentration and in the
585 crystalline state. The AFM studies reported here show that the
586 small molecule GL15 induces the formation of discrete GQ
587 complexes along the length of poly(G) molecules, whose
588 dimensions are essentially the same as those formed by
589 d(TG₄T), i.e., are indicative of short parallel-folded three-layer
590 GQs. Further studies are needed to dissect out the detailed
591 nature of these ligand complexes. The data presented here
592 suggests that appropriately selective small molecules can form a
593 number of GQ binding sites along a long length of
594 homoguanosine RNA (or DNA) sequence and has implications
595 for our understanding of the role played by GQs in cellular

596 processes in both coding and noncoding regions in a genome
597 and their perturbation by small molecule binding.

598 ■ CONCLUSIONS

599 The interactions of the GQ-targeting triazole-linked acridine
600 ligand GL15 with the short-chain length *Tetrahymena telomeric*
601 DNA repeat sequence d(TG₄T) and with the poly(G)
602 sequence have been reported here at the single-molecule
603 level, using a novel analytical approach that combines AFM and
604 voltammetry. In the presence of GL15, GQ formation was
605 detected by AFM via the adsorption of GL15-d(TG₄T)-GQ_t
606 and GL15-poly(G)-GQ small spherical aggregates and large
607 GL15-poly(G)-GQ assemblies and by DP voltammetry via
608 GL15 and G oxidation peak current decrease and disappear-
609 ance, and the occurrence of a GQ oxidation peak. The AFM
610 and voltammetric results show that the GL15 molecule
611 interacts with both sequences in a time-dependent manner.
612 An excellent correlation was observed between the d(TG₄T)
613 and poly(G) structural changes and redox behavior, before and
614 after interaction with GL15, and was directly influenced by the
615 presence of monovalent Na⁺ or K⁺ ions in solution. These
616 results are consistent with the interaction of triazole-linked
617 acridine derivatives with terminal G-quartets in an individual
618 GQ. The binding of the GL15 molecule to d(TG₄T) and
619 poly(G) both strongly stabilized the GQs and accelerated GQ
620 formation, in both Na⁺ and K⁺ ions solutions, although only the
621 K⁺-containing solution promoted the formation of perfectly
622 aligned tetra-molecular GQs. The combination of these two
623 analytical methodologies is very important to study the effect of
624 GL15 binding to GQ and will trigger their use for a whole
625 range of analysis concerning drug interactions with DNA
626 targets.

627 ■ AUTHOR INFORMATION

628 Corresponding Author

629 *E-mail: brett@ci.uc.pt.

630 Notes

631 The authors declare no competing financial interest.

632 ■ ACKNOWLEDGMENTS

633 Financial support from Fundação para a Ciência e Tecnologia (FCT),
634 Grant SFRH/BPD/92726/2013 (A.-M. Chiorcea-
635 Paquim), Project Grant (A.D.R. Pontinha), Projects PTDC/
636 SAU-BMA/118531/2010, PTDC/QEQ-MED/0586/2012,
637 PEst-C/EME/UI0285/2013, and CENTRO-07-0224-FEDER-
638 002001 (MT4MOBI) (cofinanced by the European Communi-
639 ty Fund FEDER), FEDER funds through the program COMPETE-Programa Operacional Factores de Competitivi-
640 dade is gratefully acknowledged. Work in the S.N. laboratory
641 was supported by Programme Grant No. C129/A4489, from
642 Cancer Research UK, and by the FP6 framework grant
643 "Molecular Cancer Medicine" from the EU. S.S. was a
644 Maplethorpe Fellow of The University of London.

645 ■ REFERENCES

- (1) Bochman, M. L.; Paeschke, K.; Zakian, V.A. *Nat. Rev. Genet.* 2012, 13, 770–780.
- (2) Murat, P.; Balasubramanian, S. E. *Curr. Opin. Genet. Dev.* 2014, 25, 22–29.
- (3) Neidle, S. In *Therapeutic Applications of Quadruplex Nucleic Acids*; Academic Press: Boston, MA, 2012; Chapter 2, pp 21–42.
- (4) Burge, S.; Parkinson, G. N.; Hazel, P.; Todd, A. K.; Neidle, S. *Nucleic Acids Res.* 2006, 34, 5402–5415.

- 655 (5) Du, Z.; Zhao, Y.; Li, N. *Nucleic Acids Res.* **2009**, *37*, 6784–6798.
656 (6) Eddy, J.; Maizels, N. *Nucleic Acids Res.* **2008**, *36*, 1321–1333.
657 (7) Bugaut, A.; Balasubramanian, S. *Nucleic Acids Res.* **2012**, *40*,
658 4727–4741.
659 (8) Todd, A. K.; Johnston, M.; Neidle, S. *Nucleic Acids Res.* **2005**, *33*,
660 2901–2907.
661 (9) Bugaut, A.; Balasubramanian, S. *Nucleic Acids Res.* **2012**, *40*,
662 4727–4741.
663 (10) Biffi, G.; Tannahill, D.; McCafferty, J.; Balasubramanian, S. *Nat. Chem.* **2013**, *5*, 182–186.
664 (11) Henderson, A.; et al. *Nucleic Acids Res.* **2013**, *42*, 860–869.
665 (12) Chen, Y.; Yang, D. Sequence, Stability, and Structure of G-
666 Quadruplexes and Their Interactions with Drugs. In *Current Protocols*
667 in *Nucleic Acid Chemistry*; John Wiley & Sons, Inc.: New York, 2012;
668 *50*, pp 17.5:17.5.1–17.5.17.
669 (13) Oganesian, L.; Bryan, T. M. *BioEssays* **2007**, *29*, 155–165.
670 (14) Ohnmacht, S. A.; Neidle, S. *Bioorg. Med. Chem. Lett.* **2014**, *24*,
671 2602–2612.
672 (15) Sissi, C.; Palumbo, M. *Curr. Pharm. Des.* **2014**, *20*, 6489–6509.
673 (16) Campbell, N. H.; Parkinson, G. N.; Reszka, A. P.; Neidle, S. J.
674 *Am. Chem. Soc.* **2008**, *130*, 6722–6724.
675 (17) Gunaratnam, M.; Greciano, O.; Martins, C.; Reszka, A. P.;
676 Schultes, C. M.; Morjani, H.; Riou, J.-F.; Neidle, S. *Biochem. Pharmacol.* **2007**, *7*, 679–689.
677 (18) Salvati, E.; Leonetti, C.; Rizzo, A.; Scarsella, M.; Mottolese, M.;
678 Galati, R.; Sperduti, I.; Stevens, M. F. G.; D'Incalci, M.; Blasco, M.;
679 Chiorino, G.; Bauwens, S.; Horard, B.; Gilson, E.; Stoppacciaro, A.;
680 Zupi, G.; Biroccio, A. *J. Clin. Invest.* **2007**, *117*, 3236–3247.
681 (19) Sparapani, S.; Haider, S. M.; Doria, F.; Gunaratnam, M.; Neidle,
682 S. *J. Am. Chem. Soc.* **2010**, *132*, 12263–12272.
683 (20) Collie, G. W.; Sparapani, S.; Parkinson, G. N.; Neidle, S. *J. Am. Chem. Soc.* **2011**, *133*, 2721–2728.
684 (21) Oliveira Brett, A. M.; Diculescu, V. C.; Chiorcea Paquim, A. M.;
685 Serrano, S. H. P. In *Electrochemical Sensor Analysis; Comprehensive
686 Analytical Chemistry*, Vol. 49; Alegret S., Merkoçi, A., Eds.; Elsevier:
687 Amsterdam, The Netherlands, **2007**; Chapter 20, pp 413–437.
688 (22) Corduneanu, O.; Chiorcea Paquim, A. M.; Diculescu, V. C.;
689 Fiúza, S. M.; Marques, M. P. M.; Oliveira Brett, A. M. *Anal. Chem.*
690 **2010**, *82*, 1245–1252.
691 (23) Oliveira, S. C. B.; Chiorcea Paquim, A. M.; Ribeiro, S. M.; Melo,
692 A. T. P.; Vivan, M.; Oliveira Brett, A. M. *Bioelectrochemistry* **2009**, *76*,
693 201–207.
694 (24) Chiorcea Paquim, A. M.; Corduneanu, O.; Oliveira, S. C. B.;
695 Diculescu, V. C.; Oliveira Brett, A. M. *Electrochim. Acta* **2009**, *54*,
696 1978–1985.
697 (25) Pontinha, A. R.; Alves Jorge, D. S. M.; Chiorcea Paquim, A. M.;
698 Diculescu, V. C.; Oliveira Brett, A. M. *Phys. Chem. Chem. Phys.* **2011**,
699 *13*, 5227–5234.
700 (26) Diculescu, V. C.; Chiorcea Paquim, A. M.; Eritja, R.; Oliveira
701 Brett, A. M. *J. Electroanal. Chem.* **2011**, *656*, 159–166.
702 (27) Diculescu, V. C.; Chiorcea Paquim, A. M.; Eritja, R.; Oliveira
703 Brett, A. M. *J. Nucleic Acids* **2010**, *2010*, No. 841932.
704 (28) Chiorcea Paquim, A. M.; Santos, P. V.; Oliveira Brett, A. M.
705 *Electrochim. Acta* **2013**, *110*, 599–607.
706 (29) Chiorcea Paquim, A. M.; Santos, P.; Diculescu, V. C.; Eritja R.;
707 Oliveira Brett, A. M. In *Guanine Quartets: Structure and Application*;
708 Fritzsch, W., Spindler, L., Eds.; RSC Publishing: Cambridge, U.K.,
709 2013; pp 100–109.
710 (30) Chiorcea Paquim, A. M.; Santos, P. V.; Eritja, R.; Oliveira Brett,
711 A. M. *Phys. Chem. Chem. Phys.* **2013**, *15* (23), 9117–9124.
712 (31) Chiorcea Paquim, A. M.; Oliveira Brett, A. M. *Electrochim. Acta*
713 **2014**, *126*, 162–170.
714 (32) Chiorcea Paquim, A. M.; Pontinha, A. D. R.; Oliveira Brett, A.
715 M. *Electrochim. Commun.* **2014**, *45*, 71–74.
716 (33) Pontinha, A. D. R.; Chiorcea Paquim, A. M.; Eritja, R.; Oliveira
717 Brett, A. M. *Anal. Chem.* **2014**, *86*, 5851–5857.
718 (34) Pontinha, A. D. R.; Sparapani, S.; Neidle, S.; Oliveira-Brett, A.
719 M. *Bioelectrochemistry* **2013**, *89*, 50–56.
720 (35) Laughlan, G.; Murchie, A. I.; Norman, D. G.; Moore, M. H.; Moody, P. C.; Lilley, D. M.; Luisi, B. *Science* **1994**, *265*, 520–524.
721 (36) Clark, G. R.; Pytel, P. D.; Squire, C. J.; Neidle, S. *J. Am. Chem. Soc.* **2003**, *125*, 4066–4067.
722 (37) Pagano, B.; Fotticchia, I.; Tito, S.; Mattia, C. A.; Mayol, L.; Novellino, E.; Randazzo, A.; Giancola, C. *J. Nucleic Acids* **2010**, *2010*, No. 247137.
723 (38) Lyubchenko, Y.; Shlyakhtenko, L.; Harrington, R.; Odent, P.; Lindsay, S. *Proc. Natl. Acad. Sci. U.S.A.* **1993**, *90*, 2137–2140.
724 (39) Faingold, A.; Cohen, S. R.; Shahar, R.; Weiner, S.; Rapoport, L.; Wagner, H. D. *J. Biomech.* **2014**, *47*, 367–372.
725 (40) Chiorcea-Paquim, A.-M.; Oretskaya, T. S.; Oliveira-Brett, A. M. *Biophys. Chem.* **2006**, *121*, 131–141.
726 (41) Brett, C. M. A.; Oliveira Brett, A. M.; Serrano, S. H. P. *J. Electroanal. Chem.* **1994**, *366*, 225–231.
727 (42) Mergny, J. L.; Cian, A.; Ghelab, A.; Sacca, B.; Lacroix, L. *Nucleic Acids Res.* **2005**, *33*, 81–94.
728 (43) Haider, S. M.; Parkinson, G. N.; Neidle, S. *J. Mol. Biol.* **2003**, *326*, 117–125.
729 (44) Campbell, N. H.; Parkinson, G. N.; Reszka, A. P.; Neidle, S. *J. Am. Chem. Soc.* **2008**, *130*, 6722–6724.
730 (45) Dai, J.; Carver, M.; Hurley, L. H.; Yang, D. *J. Am. Chem. Soc.* **2011**, *133*, 17673–17680.
731 (46) Arnott, S.; Chandrasekaran, R.; Marttila, C. M. *Biochem. J.* **1974**, *141*, 537–543.
732 (47) Sengar, A.; Heddi, B.; Phan, A. T. *Biochemistry* **2014**, *53*, 7718–7723.
733 (48) Sengar, A.; Heddi, B.; Phan, A. T. *Biochemistry* **2014**, *53*, 7718–7723.
734